Biomineral Amorphous Lasers through Light-Scattering Surfaces Assembled by Electrospun Fiber Templates

Maria Moffa, Andrea Camposeo, Vito Fasano, Barbara Fazio, Maria Antonia Iatì, Onofrio M. Maragò, Rosalba Saija, Heinz-Christoph Schröder, Werner E. G. Müller, and Dario Pisignano**

New materials aim at exploiting the great control of living organisms over molecular architectures and minerals. Optical biomimetics has been widely developed by microengineering, leading to photonic components with order resembling those found in plants and animals. These systems, however, are realized by complicated and adverse processes. Here we show how biomineralization might enable the one-step generation of components for amorphous photonics, in which light is made to travel through disordered scattering systems, and particularly of active devices such as random lasers, by using electrospun fiber templates. The amount of bio-enzymatically produced silica is related to light-scattering capacity and the resulting organosilica surfaces exhibit a transport mean free path for light as low as 3 μm, and lasing with linewidth below 0.2 nm. The resulting, complex optical material is characterized and modelled to elucidate scattered fields and lasing performance. Tightly-controlled nanofabrication of direct biological inspiration establishes a new concept for the additive manufacturing of engineered light-diffusing materials and photonic components, not addressed by existing technologies.

1. Introduction

Nature represents an unlimited font of inspiration for the development of novel materials. The exceptional control that living organisms exert over the composition, structure and morphology of many compounds and minerals, the generally mild conditions required to physiologically form these materials, as well as their resulting physical properties may enable smart applications in optics and photonics.[1–4] Two concepts are being developed in this framework. The first involves optical biomimetics through microengineering, namely using or mimicking photonic crystals, anti-reflectors, iridescent structures or other resonators found in many plants and animals.[4–6] The second option relies on the elaboration of manufacturing processes of true biological derivation, namely on the emulation of natural nanofabrication mechanisms, which might involve genetic encoding, specific peptide sequences, or proteins directing the polycondensation of mineral precursors.[7–12] Most often, however, the structures produced *in-vitro* are very far from reaching the richness and the optical functions of natural archetypes.

To achieve truly complex optical materials by biomineralization, it is important to take as much advantage as possible of the characteristic features which are inherent to natural biophotonic structures. These systems are generally *disordered* to some extent, and minerals in them are frequently incorporated in branched microenvironments with low-refractive index ($n \sim 1.5$) compounds, and templated by fibrillar protein architectures in the extracellular matrices. All these properties might address biomineralization in an effective way to realize surfaces and

M. Moffa, A. Camposeo, D. Pisignano
NEST
Istituto Nanoscienze-CNR
Piazza S. Silvestro 12, I-56127 Pisa, Italy
E-mail: andrea.camposeo@nano.cnr.it; dario.pisignano@unisalento.it
V. Fasano, D. Pisignano
Dipartimento di Matematica e Fisica "Ennio De Giorgi"
Università del Salento
via Arnesano, I-73100 Lecce, Italy
B. Fazio, M.A. Iatì, O.M. Maragò
CNR-IPCF
Istituto Processi Chimico-Fisici
Viale F. Stagno D'Alcontres, 37, I-98158 Messina, Italy

R. Saija
Dipartimento di Scienze Matematiche e Informatiche
Scienze Fisiche e Scienze della Terra
Università di Messina
Viale F. Stagno d'Alcontres 31, I-98166 Messina, Italy
H.-C. Schröder, W. E. G. Müller
Institute for Physiological Chemistry
University Medical Center of the Johannes Gutenberg University
Duesbergweg 6, D-55128 Mainz, Germany

The ORCID identification number(s) for the author(s) of this article can be found under https://doi.org/10.1002/lpor.201700224

DOI: 10.1002/lpor.201700224

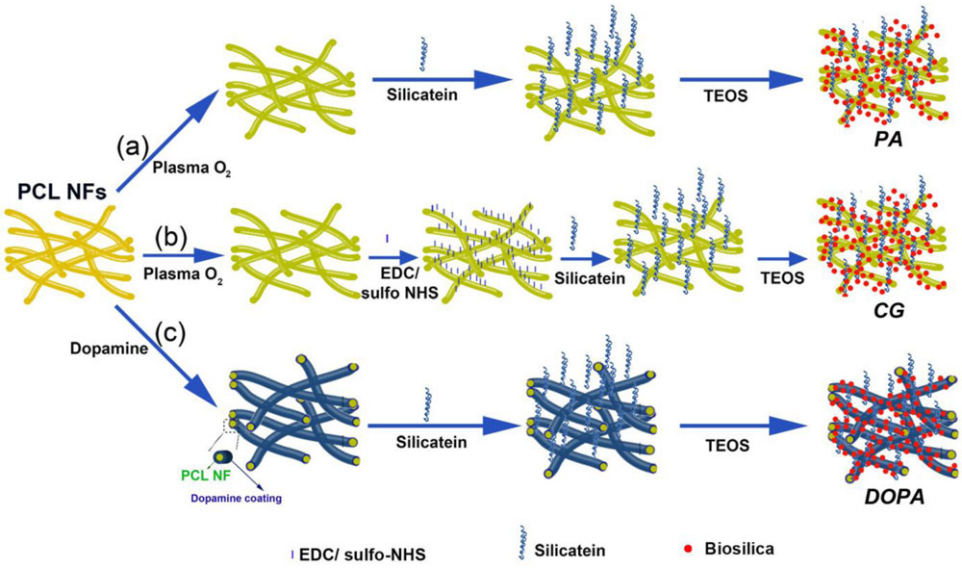

Figure 1. Schematics of the stepwise silicatein-coating of nanofibers and production of biosilica over large-area templates. (a) *PA*, (b) *CG* and (c) *DOPA* functionalization.

devices for amorphous photonics, exploiting multiply scattered light in disordered structures.[13] For instance, sponges and diatoms are known to synthesize nano-structured silica, by means of special classes of proteins.[2,9–14] Silica is widely used in optics, although its artificial production usually involves high temperature and harsh chemical conditions. Among potential applications of silica nanostructures in amorphous photonics, so-called random lasers[6,15,16] have attracted great attention due to the technological potential of these low-cost light sources for medicine and spectroscopy,[13] and to the wealth of physical effects occurring when light travels through disordered systems, which include coherent back-scattering (CBS)[16–18] and formation of random resonators in gain materials.[16,19]

Here we report on random laser devices realized by biomineralization. Light-diffusing organosilica fibers at the base of the laser formation are obtained by a straightforward method. We developed and compared different surface functionalization strategies of the silicatein protein onto electrospun fibers, followed by *in-vitro* biosilicification. The capacity of building effective light-scattering surfaces is found to be promoted by silica particles at a specific spatial density. The resulting hybrid material incorporated with an organic dye shows random lasing spikes with a spectral linewidth smaller than 0.2 nm and a threshold fluence of 7.5 mJ cm^{-2}.

The importance of this method stands in various aspects. Firstly, the possibility is opened to direct the realization of functional components for amorphous photonics by cheap and gentle, bioinspired approaches, mimicking the routine assembly of micro-structures that is performed in nature. Secondly, the approach combines the advantages of large-area fiber spinning and biomineralization, thus establishing more versatile design rules for the development of photonic structures. The resulting, silica-fibers hybrid devices exhibit a transport mean free path of light, (3.3 ±0.2) μm, comparable with the smallest values so far reported for low-n materials, which is reflected in a threshold for random lasing smaller than those of other organic solid-state systems.

2. Experimental Methods and Materials

2.1. Materials

Silicatein-α cDNA from *S. domuncula* is inserted into the oligo-histidine expression vector pQ30 (Qiagen), transforming *E. coli* host strain Novagen BL 21 (Merck) with this plasmid and harvesting it in a BIOSTAT Aplus bioreactor (Sartorius Stedim Biotech). Isopropyl β-D-1-thiogalactopyranoside is added to induce the expression of the fusion protein, and the recombinant protein is finally collected, purified by affinity chromatography and refolded. Other chemicals are obtained from Sigma Aldrich, unless otherwise specified.

2.2. Electrospinning and Biosilica Synthesis

Solutions with concentration of 200 mg/mL are prepared by dissolving polycaprolactone (PCL, average Mn 80,000) in a dichloromethane:dimethylformamide mixture (80:20 v/v) under stirring for 12 h at room temperature. For carrying out electrospinning the solution is loaded in a 1 mL plastic syringe and injected through a stainless-steel blunt needle using an infusion pump (Harvard Apparatus) at an injection rate of 0.5 mL·h^{-1}, with an applied voltage of 5 kV (EL60R0.6-22, Glassman High Voltage). Fibers are collected at a distance of 10 cm from the needle tip, at air humidity of about 45% and temperature of 20°C, and stored under vacuum at room temperature. Fiber functionalization is performed according to the processes schematized in **Figure 1**. For methods based on physisorption (*PA*) and chemical grafting (*CG*), fibers are firstly treated with plasma oxygen by a tabletop system (Tucano, Gambetti Kenologia) at 30 W for

3 min. Afterwards, fibers are incubated in a 50 μg/mL silicatein solution for 3 hours. For *CG*, samples are also treated with 10 mM 1-ethyl-3-(3-dimethylaminopropyl)carbodiimide hydrochloride (EDC) and 20 mM *N*-hydroxysulfosuccinimide for 1 hour at room temperature prior to protein incubation. For functionalization with polydopamine coatings (*DOPA*), fibers are firstly immersed in 2 mg/mL dopamine, 10 mM Tris-HCl (pH 8.5) with gentle shaking for 24 h at room temperature, followed by washing with water to remove unbound dopamine. Samples are then transferred into silicatein solutions (50 μg/mL) for 3 h. Pristine PCL fibers are used as negative control. A QuantiPro bicinchoninic acid (BCA) Assay Kit is used to investigate the amount of adsorbed silicatein, measuring absorbance at 562 nm by a spectrophotometer (Lambda 950, Perkin Elmer Inc.). As reference, a 6 points standard curve in triplicate is calculated using silicatein solutions. Each quantification measurement is repeated on at least ten normally identical samples. The concentrations per unit surface area (μg cm^{-2}) of protein immobilized onto different surfaces are so calculated. Horizontal attenuated total reflectance-Fourier transform infrared (HATR-FTIR) spectroscopy is carried out by a Spectrum 100 system (Perkin Elmer Inc.), with 2 cm^{-1} resolution and utilizing a ZnSe 45-degree flat-plate. Spectra are baseline-corrected and smoothed. To analyze the protein secondary structure, the second-derivative of spectra are calculated and then fitted with Gaussian band profiles. Fluorescein isothiocyanate (FITC) in dimethyl sulfoxide is used to investigate the silicatein distribution by confocal laser scanning microscopy. To this aim, a bicarbonate buffer ($NaHCO_3$ solution *A*; 3.5 mL, 0.1 M) is mixed with carbonate buffer (Na_2CO_3 solution *B*; 315 μL, 0.1 M), samples are incubated in *A*+*B* (1.3 mL) with addition of FITC/dimethyl sulfoxide solution (100 μL, 1.5 mg/mL), at 4°C for 8 hours. Afterwards, they are washed 3 times with phosphate buffer solution (5 minutes each) and observed by an inverted microscope (Eclipse Ti) equipped by a confocal A1 R MP system (Nikon). Silicatein-bound fibers are incubated in tetraethoxysilanes (TEOS, purity ≥ 99.0%) at room temperature, for times up to 5 days. After 1, 3 and 5 days samples are washed with ethanol and inspected. The morphology and composition of obtained biosilica is evaluated by scanning electron microscopy (SEM) and energy dispersive X-ray (EDX) analysis (FEI). To evaluate the average distance between silica particles, the WSxM software package[20] is used to analyze the SEM images.

2.3. Random Lasing Devices

Biosilicificated fibers are coated with a film of polyvinylpyrrolidone (PVP, Alfa Aesar, Mn 130,000) doped with disodium-1,3,5,7,8-pentamethylpyrromethene-2,6-disulfonate-difluoroborate complex (pyrromethene, stimulated emission cross-section, $\sigma_{se} \cong 10^{-19}$ cm^2, see Supporting Information). The solution is obtained by 30 mg/mL of PVP and 3 mg/mL of pyrromethene in water with sonication for 2 h, and drop-cast onto fibers, up to complete water evaporation at room temperature (~ 2 days). Light-diffusing surfaces are then excited by the third harmonic of a pulsed Nd:YAG laser ($\lambda_{exc} = 355$ nm, repetition rate = 10 Hz, pulse duration = 10 ns). The excitation laser beam is focused on the samples in a stripe shape (2 mm × 150 μm), and precisely aligned on one edge of the samples by means of a micrometric translation stage. The emission signal is collected from the excited edge of the sample by a lens and coupled to an optical fiber. The spectral features of the collected emission are analysed by a monochromator, equipped with a charge coupled device (CCD) detector. The samples are mounted in a vacuum chamber and all measurements are performed in vacuum ambient (pressure < 10^{-4} mbar) in order to minimize degradation effects due to photo-oxidation.

2.4. Characterization of Light Transport Properties in the Fiber-Biosilica System

CBS experiments are performed by a continuous wave He-Ne laser source ($\lambda = 633$ nm), a system of lenses, a cube beam-splitter, a $\lambda/4$ waveplate and a polarization filter, and by determining angular profiles of the intensity backscattered from samples by a CCD. For fitting CBS data, we set a slab thickness of 200 μm, and the inelastic mean free path (1700 μm) is calculated for effective media given by either 22%/78% PCL/air or 22%/2%/76% PCL/silica/air, mimicking actual samples. A finite slab model is used to fit CBS data and determine the transport mean free path for light. Light-scattering in the fiber-biosilica hybrid materials at 355 nm and at 570 nm is studied by field expansion in terms of spherical multipole fields and calculating the T-matrix for clusters of spheres encompassing linear aggregates to describe nanofibers.

3. Results and Discussion

3.1. Biomineralized Surfaces on Electrospun Fiber Templates

A platform of different techniques is implemented in this work to functionalize electrospun PCL fibers with silicatein (Figure 1), including *PA*, *CG* and *DOPA* methods. Aspecific, *PA*-functionalization is performed by direct incubation in the protein solution (Figure 1a), whereas EDC and sulfo-*N*-hydroxysulfosuccinimide are used as zero-length crosslinker and catalyst for *CG*, respectively (Figure 1b). Such coupling procedure immobilizes proteins onto supports without introducing spacing arms. Finally, polydopamine coatings on PCL are realized to subsequently immobilize silicatein by simple dipping (Figure 1c). This method, based on the oxidative polymerization of dopamine, lacks of complicated process steps and of possible cleavage of polymer chains, thus potentially overcoming a few important drawbacks of common surface modifiers.[21]

The amount of protein adsorbed on the electrospun templates is then estimated by labeling fiber-bound silicatein with FITC for confocal laser scanning microscopy, evidencing a more uniform distribution and a higher amount of proteins along fibers undergone *CG* and *DOPA*-treatments (**Figure 2**a–h and Figure S1 in the Supporting Information). These results are supported by quantification by a BCA assay (Figure 2i). *CG* and *DOPA*-methods allow significantly higher amount of immobilized protein to be found (22-23 ± 2 μg/cm^2) compared to *PA* (5±1 μg/cm^2). However, we point out that the bare amount of immobilized protein does not necessarily indicate what is the

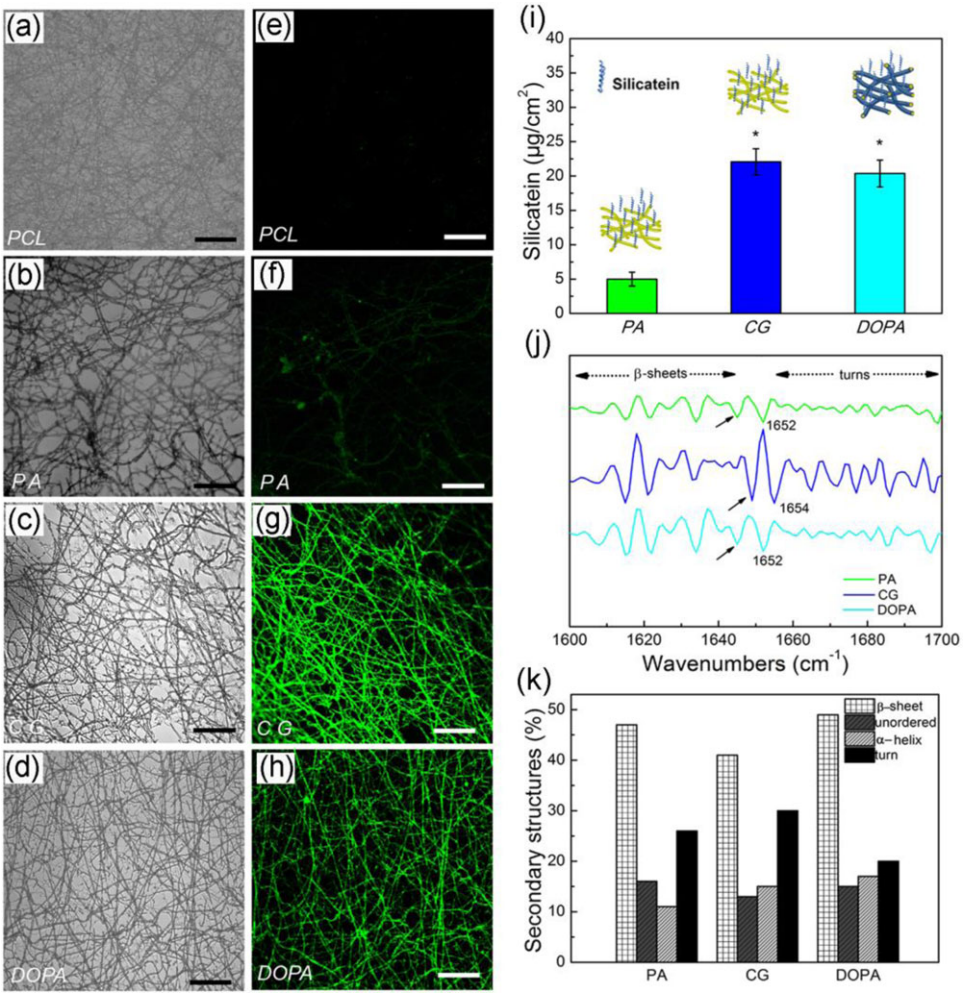

Figure 2. Recombinant silicatein on electrospun templates. Optical transmission (a-d) and fluorescence (e-h) micrographs of FITC-labeled silicatein, immobilized on PCL fibers by physisorption (*PA*, b, f), chemical grafting (*CG*, c, g) and polydopamine (*DOPA*, d, h). (a) and (e): pristine PCL fibers treated with FITC, used as control. (i) Quantification of immobilized silicatein on electrospun templates by the different functionalization methods. Results are expressed as (mean ± standard deviation). Asterisks show statistically significant differences compared to *PA* ($P < 0.05$). The cartoons above each column show the different samples. Vertical helices and fiber sheaths schematize silicatein and the dopamine coating, respectively. (j, k) Secondary structure analysis of silicatein adsorbed on nanofibers. (j) Second derivative FTIR spectra of the amide I region, for silicatein-functionalized fibers by physisorption (*PA*, top, green curve), chemical grafting (*CG*, middle, blue curve) and polydopamine (*DOPA*, bottom, cyan curve). (k) Corresponding percent quantification of β-sheet, unordered, α-helix and turns secondary structures of silicatein.

best functionalization method in terms of leading to effectively light-scattering surfaces. In particular, a higher amount of immobilized proteins does not necessarily result in better-suited biosilicificated mats for random lasing, as will be assessed in the following.

To investigate the surface-silicatein interactions more in depth, we study the different samples by HATR-FTIR spectroscopy (Figure S2). Characteristic infrared bands for PCL-related stretching modes are notable for pristine PCL, polydopamine-treated PCL (PCL*, without silicatein), and silicatein-functionalized fibers (*PA*, *CG* and *DOPA* samples), with the latter also showing peaks at 3300 cm^{-1} (1 in Fig. S2), 1650 cm^{-1} (2) and 1560 cm^{-1} (3), attributable to amide A, amide I and amide II, respectively. The silicatein secondary structure can be analyzed by the shape of the amide I band. To this aim, the relative areas of the overlapping band components under the amide I contour are resolved and quantified through their second-derivative (Figure 2j), in combination with Gaussian curve-fitting analysis.[22] Bands at 1693, 1639, and 1628 cm^{-1} are to be assigned to β-sheets, the band at 1652 cm^{-1} to an α-helix, bands at 1684, 1671, and 1663 cm^{-1} to turns, and the band at 1645 cm^{-1} to an unordered structure, respectively.[23] The quantification of these bands (Figure 2k) evidences for polydopamine and *PA*-methods higher levels of secondary structures, associated to the presence of active silicateins. These features, related to the different reactivity of fibers toward proteins and to consequent conformational changes of silicateins, are likely to affect the resulting bioenzymatic activity. Taken together, these results highlight polydopamine-mediated functionalization as optimal approach ensuring both high amounts of proteins linked to electrospun templates and enhanced bands associated to pristine secondary structures.

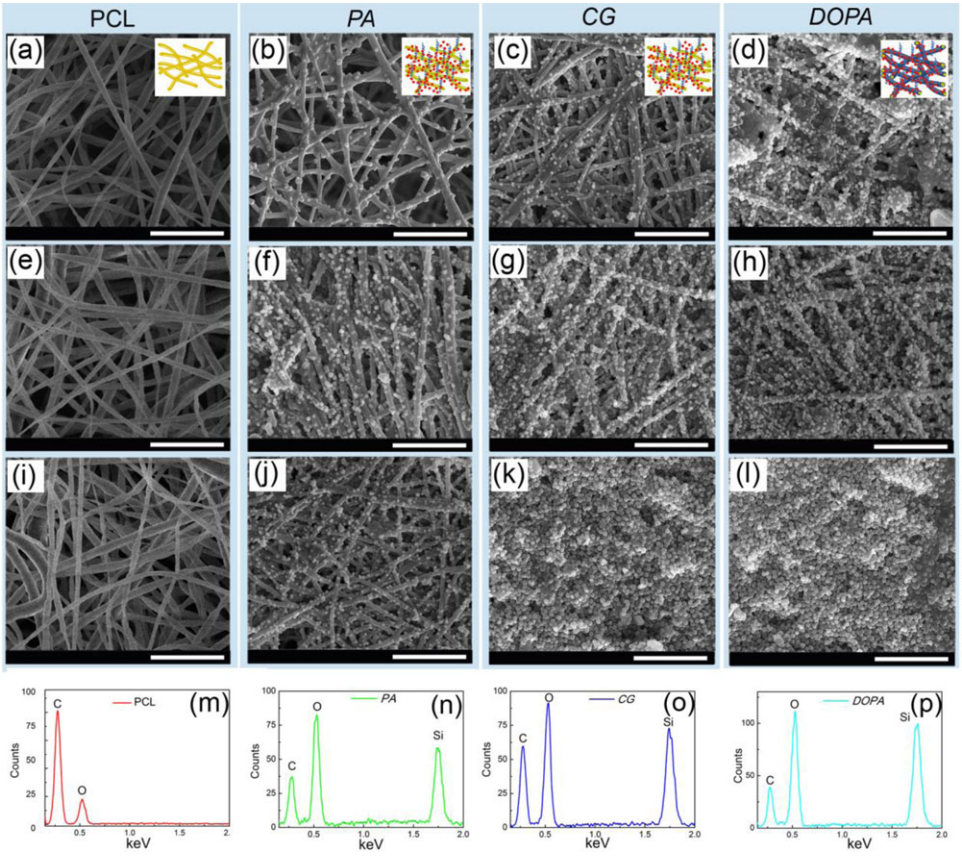

Figure 3. Synthesis of biosilica spheres on silicatein-functionalized spun fibers. SEM micrographs of samples obtained by *PA* (b, f and j), *CG* (c, g and k) and polydopamine (*DOPA*, d, h and l), after various days of incubation in TEOS. (a), (e) and (i) micrographs show pristine PCL fibers as control. Fibers are incubated for 1 day (a-d), 3 days (e-h) and 5 days (i-l), respectively. Scale bar = 5 μm. (m-p) Corresponding EDX spectra after 5 days of incubation, for PCL fibers (m), and for samples undergone *PA* (n), *CG* (o) and polydopamine treatment (p). The top-right insets in each column show sample schematics. Vertical helices: silicatein. Fiber sheaths: dopamine coating. Red dots: biosilica.

Spun templates, including uncoated samples as control, are then incubated with TEOS at ambient conditions. The resulting formation of biosilica on protein-functionalized samples is directly observable by SEM performed at different time steps of incubation (**Figure 3**). No deposits are appreciable on pristine PCL fibers even after five days (Figure 3a, e and i). Instead, on silicatein-functionalized fibers, silica spheres with diameter up to 300 nm start to precipitate during the first day of TEOS incubation (Figure 3b–d). The density of spheres found on *PA*-samples after 1 day and 5 days is of about 1.5×10^6 particles/mm^2 and 4×10^6 particles/mm^2, respectively. A relatively higher density is observed on *CG* and *DOPA*-samples (i.e. $\sim 3.5 \times 10^6$/mm^2 and 6×10^6/mm^2 after 1 day). Upon increasing the incubation time, the area covered by biosilica increases as well, up to completely covering *CG* and *DOPA*-samples with a continuous film (Figure 3k and l). The different amount of deposited silica will have a strong impact on the resulting lasing properties of these surfaces, as described below. In addition, EDX analysis of the synthetized material gives evidence that it consists of silica, whereas no silica is formed on pristine fibers incubated in the absence of silicatein (Figure 3m–p). Finally, silica particles are quite uniform. For instance, those formed on *PA*-samples are regular spheres with average diameter about 180 nm. These results are in agreement with previous studies on histidin-tagged silicatein catalyzing the formation of interconnected silica nanospheres with a diameter up to 300 nm,[24] and are well consistent with *in vivo* biosilicification in sponges, in which spicules formation is initiated by the synthesis of silica granules with size of 100–600 nm.

3.2. Random Lasers

Surfaces embedding wavelength-scale spheres can be excellent diffusing elements leading to random lasers, depending on the degree of surface coverage. **Figure 4** and Figure S3 summarize the emission properties of the various biosilicificated surfaces under ns-pulsed excitation, following the deposition of a film of PVP doped with pyrromethene. In particular, in Figure 4 we compare (i) devices where only electrospun (PCL) fibers are used in addition to the dye-doped polymer supporting optical gain, with (ii) devices where fibers are coated with biomineralized silica spheres prior dye-doped polymer casting. The two devices are therefore identical in their fibrous geometry underneath and gain material, namely their eventually different spectral and threshold behavior is directly related to the presence of additional scattering from silica spheres, at a well-defined surface density, in

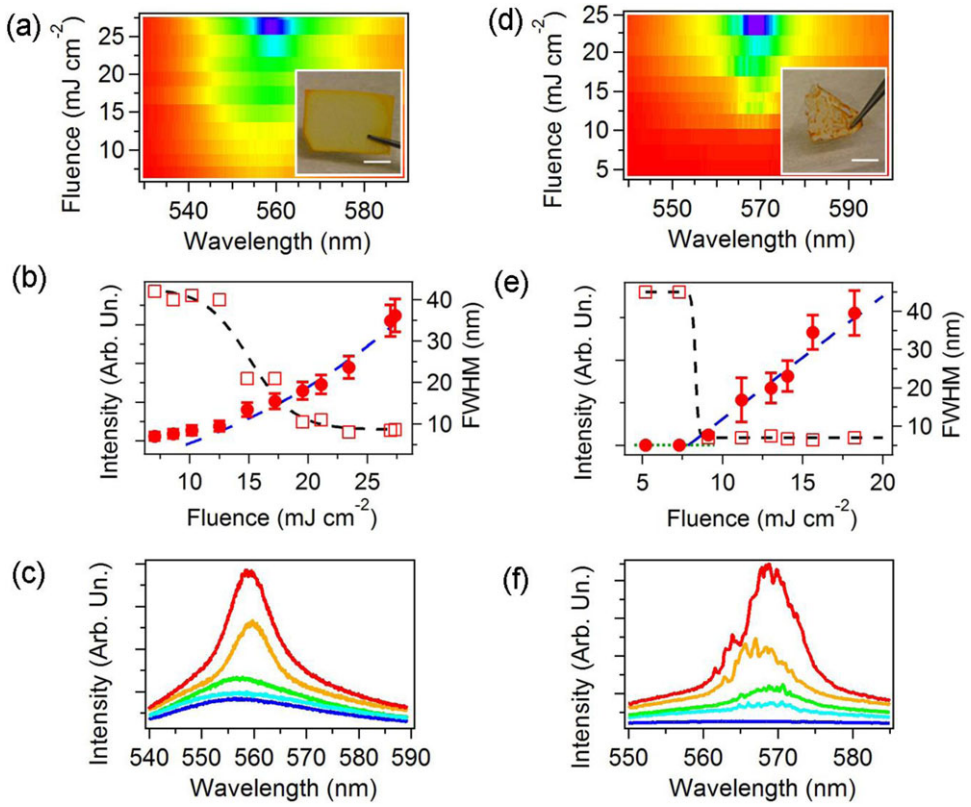

Figure 4. Random lasing of organosilica surfaces. Analysis of the emission properties, under pulsed excitation, of devices realized on PCL fibers (a-c), and *PA* dye-doped devices (d-f), respectively. (a), (d): Emission intensity maps showing the spectra of the samples as a function of the excitation fluence. Insets: corresponding device photographs. Scale bars = 5 mm. (b), (e): Intensity (left vertical axis) and spectral line-width (right axis) of the emission *vs.* excitation fluence. The blue dashed lines in (b) and (e) are fits to intensity data by an exponential-like law and by an above-threshold linear curve, respectively. The black dashed lines are guide to the eye for line-narrowing data. (c), (f): Emission spectra collected at increasing excitation fluences. Shown curves are averages of many single-shot emission spectra. From bottom to top, excitation fluences: (c): 8, 12, 14, 23, 27 mJ cm^{-2}; (g): 5, 11, 14, 18, 23 mJ cm^{-2}.

biomineralized samples. Therefore, this comparison is highly useful in view of elucidating the working mechanisms of the random laser. Figure 4a and d, and Fig S3a and d display the intensity maps showing emission spectra as a function of the excitation fluence, for pristine PCL fibers, *PA*, *CG* and *DOPA* samples (photographs are in the corresponding insets, and highlight a quite different morphology even at macroscale). What is found is that in pristine PCL, as well as in *CG* and *DOPA* samples, emission line-narrowing occurs upon increasing the excitation fluence above roughly 10, 23 and 34 mJ cm^{-2}, respectively, with a smooth transition across a range of 5–10 mJ cm^{-2} as typical of amplified spontaneous emission (ASE, Figure 4b and Fig. S3b,e). In these samples the emission intensity (I) has a nonlinear, threshold-less dependence on the excitation density, which is well described by an exponential-like relation as expected for ASE. Overall, these systems exhibit good optical gain (up to tens of cm^{-1}). However, even *CG* and *DOPA* devices lack of the effective feedback mechanism needed for lasing, due to the formation of the continuous and dense layer of silica spheres. Such layer favors the waveguiding of the spontaneous emission along the organic layer, and the occurrence of ASE-related gain narrowing instead of random lasing.

PA-samples, which features a less dense population of silica microspheres compared to the other functionalized surfaces, show a different behaviour. Upon increasing the excitation fluence, a peak centred at about 569 nm and with linewidth of a few nm features a threshold behaviour (Figure 4e and f). Such threshold (7.5 mJ cm^{-2}) can be easily determined by considering the linear dependence of the emission intensity on the excitation fluence above threshold. In addition, a sharp line-narrowing transition is found at threshold. Under single-shot excitation, the laser shows a complex dynamics, with the spectral position of appreciable narrow peaks whose spectral position may vary at each pumping pulse[15] (**Figure 5**a). Additional spikes are also visible on the top of the smooth peak in Figure 4a, and show a sharp linewidth reduction down to 0.2 nm (full width at half maximum) at threshold (Figure 5b), as estimated by subtracting the underlying broader spectral background.

The comparison of excitation threshold performance shown in different studies on random lasers is made very hard by its dependence on experimental parameters such as the area of the excited region on samples. However, here found threshold values are lower than those of other random lasers based on low-n, organic systems, such as biopolymers embedding

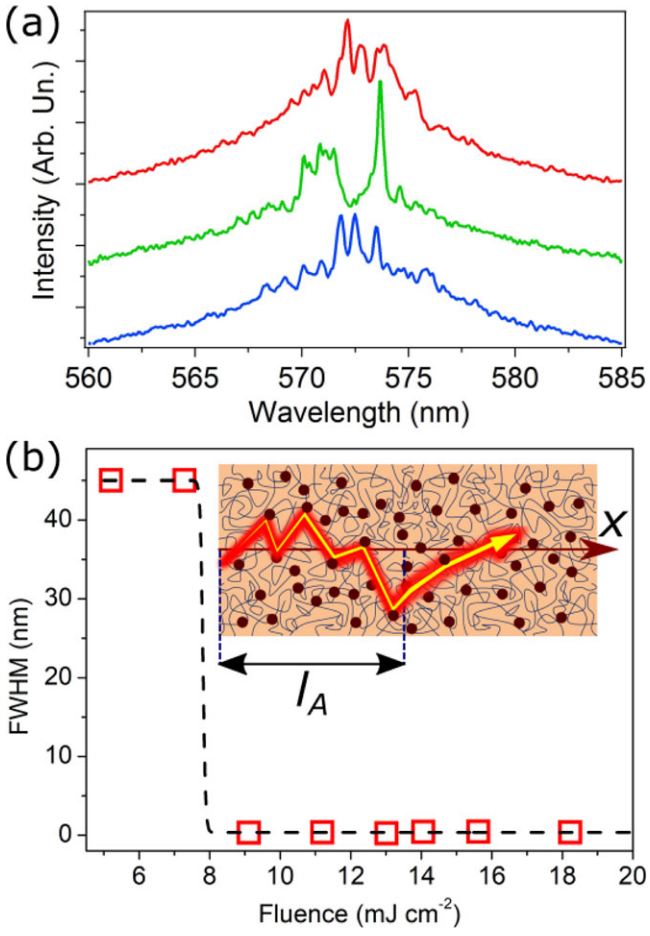

Figure 5. (a) Examples of single-shot random lasing spectra from *PA* dye-doped materials. Spectra are shifted vertically for better clarity. (b) Line-narrowing of random lasing spikes on the top of the intensity-feedback mode. The black dashed line is a guide to the eye. Inset: Schematics of the working device, through non ballistic, diffusive regime along the hybrid material. The coloured background stands for the active material. Dark wires: electrospun template fibers. Dark dots: biosilica particles. *x*: main propagation axis for stimulated emission, provided by the length of the excitation stripe. l_A: amplification length in the disordered medium, corresponding to an enhancement of the optical signal by a factor *e*. $l_A \cong 30$ μm in our system.

non-linear chromophores,[25] and are in line with recently reported, plasmon-enhanced hybrid architectures, such as dye-doped fibers incorporating Au nanoparticles,[26] and polymer films on three-dimensional nanorod metamaterials.[27] The working mechanisms of random lasing supported by the biomineralized surface involve two different effects as schematized in the inset of Figure 5b, namely stimulated emission from the active material as well as scattering from light-diffusing components. The active material is located in the dye-doped PVP layer and, in absence of significant scattering of generated light, would produce ASE supported by waveguiding along this organic slab as commonly found in light-emitting organic semiconductor films.[28,29] The thickness of the active layer is an important parameter, which when above a cut-off value (t_C) supports modes at a given wavelength (λ), $t_C = \lambda \times \{\arctan [(n_S{}^2\text{-}1)/(n^2\text{-}n_S{}^2)]^{1/2}\}/[2\pi (n^2\text{-}n_S{}^2)^{1/2}]$, where n and n_S are the refractive indexes of the dye-doped PVP and of the biomineralized material, respectively. For our system, $t_C \cong 500$ nm. When biomineralization occurs and silica particles are achieved at a given density, additional effects take place in the device. On one side, electrospun fibers can also guide coupled emitted light along their londitudinal axis,[30] namely along random directions. More importantly, significant light-scattering might take place, in principle due to both electrospun fibers and silica particles. The contribution from individual fibers in diffusing light far from the pristine propagation direction can be estimated to be small. Indeed, the calculation of the angular dependence of the light-scattering form factor for polymer fibers,[31] highlights that most of the incident light is scattered at forward angles ($\leq 40°$) when, as in our case, ka is comparable or larger than unity, where a is the fiber radius and $k = 2\pi/\lambda$ is the wavevector. Electrospun PCL filaments therefore do not substantially diffuse emitted light at large angles, which is also supported by the ASE-like emission features found for the device realized on pristine PCL fibers (Figure 4b and c). Biosilica particles, instead, more significantly affect the transport of light and hence the overall emission. The average distance between first-neighbour particles is especially relevant in this respect. When such distance is at least 280 nm, as in *PA*-samples, a well-defined threshold is found to exist for random lasing (Figure 4e). Instead, line-narrowing is observed at excitation fluences higher by 3 to 5 times (up to about 45 mJ cm^{-2}, Fig. S3b,e) when the inter-particle separation becomes lower than 250 nm and ultimately leads to densely-packed biosilica spheres, arranged in a continuous layer, as in *CG* and *DOPA*-samples. In a whole, these findings indicate a quite weak effect of light-scattering from fibers at the lasing wavelength, with a much more relevant role played by scattering from silica particles, and also suggest that the interface between the active film and the scattering surface is highly important to provide the refractive index contrast and the enhanced fields needed for lasing.

The light propagation in the hybrid material is clearly non-ballistic,[32] the excited sample size ($> 10^2$ μm) being much larger than the average distance travelled by photons between consecutive scattering centers (inset of Figure 5b). This leads to an amplification length, l_A, in the device, much shorter than the gain length (l_G) in the active material, since multiple scattering might shorten the distance along the propagation direction over which the light is amplified in an effective way. In our system, l_G is of the order of a few hundreds of μm as found by ASE measurements (Supporting Information), whereas l_A is roughly given by $(l_G\, l_T)^{1/2}$ and can also be estimated from the transport mean free path, l_T.

3.3. Light-Scattering Properties

To better assess light transport properties and estimate the transport mean free path provided by the biomineralized material, the random lasing, hybrid *PA*-system is studied both experimentally and theoretically and compared to those of pristine networks of PCL fibers. Firstly, the intensity of back-scattered light from 200 μm thick samples is measured by irradiating the diffusing material by a He-Ne laser. We then analyze the CBS cones, which describe the ratio of the total scattered light intensity to the diffuse background as a function of the angle, θ, defined by the

incoming and the outgoing light wavevectors. An enhanced reflectance is expected at small θ values following constructive interference of light along time-reversed optical paths and related to weak localization of light.[17] The here measured enhancement factor (A_{CBS}) at the exact backscattering direction due to interference in the complex material is lower than the theoretical value of 2 due to possible residues of single scattering events and stray light. Furthermore the slight decrease of A_{CBS} following silica deposition could suggest the incipient occurrence of recurrent multiple scattering events, folded and loop, in the stronger scattering material. Experimental CBS data are shown in **Figure 6**a, and evidence a larger CBS cone, namely a shorter transport mean free path for light (larger scattering strength), in fibers with silica particles. Data are well fitted by the function, $I(\theta) = [1 + (A_{CBS} -1)(\gamma_C / \gamma_L)]$ (Supporting Information), where γ_C and γ_L are the θ-dependent coherent and the diffuse background intensities for a finite slab, respectively, expressed in terms of the measured fluxes of photons per solid angle and per probed area normalized to the incident fluxes (so-called bistatic coefficients).[33] The silica-fibers hybrid structure exhibits a transport mean free path of light as low as (3.3 ± 0.2) μm, comparable with the smallest values for low-*n* materials found in dense fibrillar chitin.[34] This would lead to a l_A value of about 30 μm, which indicates the effectiveness of the amplification mechanism promoted by the light-scattering surface.

These data are indicative of specific light transport properties in the hybrid structure composed of organic fibrils and silica particles. Such complex material encompassing highly elongated filaments is hard to depict as made by isotropic scatterers. Therefore we develop a model for the scattering of light by the transition matrix (T-matrix) technique,[35] describing fibers as randomly-directed linear aggregates of 430 nm spherical building blocks (Figure 6b), and adding silica particles with 180 nm diameter (Figure 6c) as in *PA*-samples (details in Supporting Information). Biomineralization is very advantageous to this aim, since this method allows for overcoming most of the issues of etched and ground materials in terms of poorly defined shapes of scattering elements[15] and to achieve well-defined single-particle scattering properties.[17] Furthermore, being particles directly formed on the fiber template, uncontrolled clustering due to van der Waals or electrostatic forces in solution is avoided, which also simplifies modelling. Hence, we calculate the maps of scattered field normalized to an unpolarized incident field intensity ($|E_S/E_0|^2$), at both the emission (570 nm, Figure 6d and e), and the excitation (355 nm, Figure 6f and g) wavelength. The hybridization with silica nanoparticles is clearly observed to lead to strong scattering, which can be accounted by a better match between the silica particle size and the incident wavelengths.[35] At the same time, organic filaments support fields at the emission wavelength (Figure 6d) while having a much weaker effect on the excitation which is almost uniformly spread over the sample plane (Figure 6f). The resulting hot spots, namely enhanced local fields in the *PA*-material suggest more effective excitation of chromophores (Figure 6g) as well as higher overall feedback which is directly related to the occurrence of lasing at about 570 nm (Figure 6e). Analogous results are found for any direction of incoming light at the emission wavelength across the material (Figure S4). Finally, the system is effective in distributing scattered pumping fields about 1 μm deep into the sample, thus

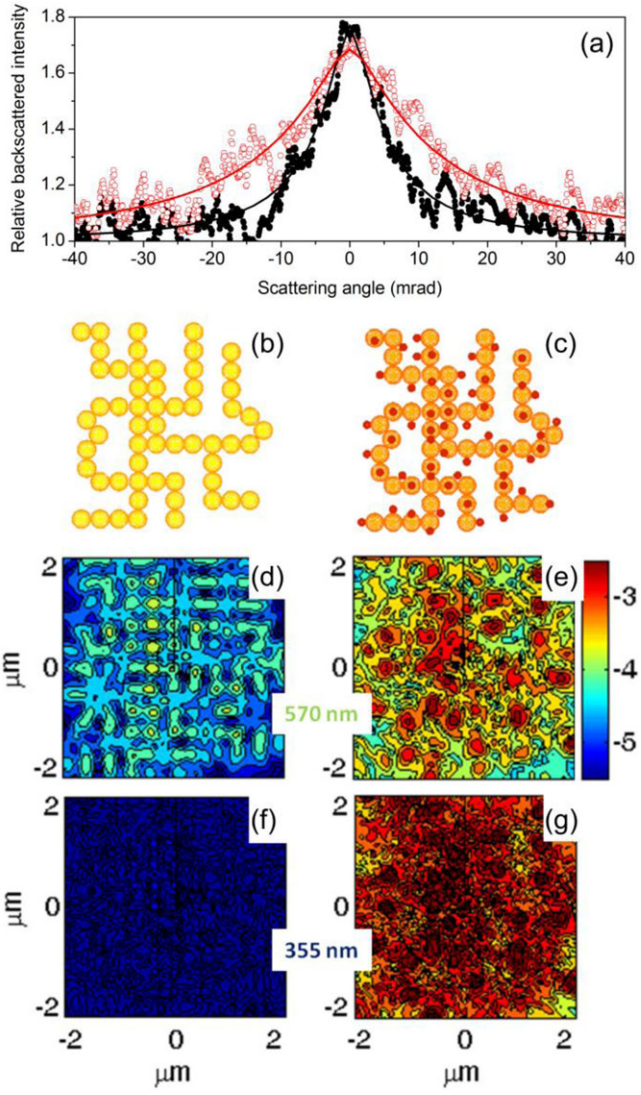

Figure 6. Light transport in organosilica material. (a): Experimental CBS data, for pristine PCL fibers (black full dots) and for *PA*-samples (red open dots), and corresponding fits (see the text). Fibers: $A_{CBS} = 1.77$, transport mean free path = (8.3 ± 0.3) μm. *PA*-samples: $A_{CBS} = 1.68$, transport mean free path = (3.3 ± 0.2) μm. Inelastic mean free path for fitting curves: 1700 μm. The absorption of silica is negligible and it does not affect the inelastic mean free path. (b, c): Models adopted for light scattering computation for the nanofiber mats (b) and for the hybridized nanofiber-biosilica structures (c). Filaments and particles are embedded in PVP as external medium. (d-g): Normalized intensity maps, $|E_S/E_0|^2$, of the scattered field for the fiber mats (d) and for the hybridized structure (e) at the emission wavelength, 570 nm (logarithmic scale). Normalized intensity maps of the scattered field for the fiber mats (f) and for the hybridized structure (g) at the excitation wavelength, 355 nm.

providing ample space for exciting surrounding dyes (Figure S5). This result supports the importance of the interface between the active material and the scattering surface, which directly involves only the top layers of the fibrous template, and the biomineral component which is there deposited. In this respect, having separated light-scattering and emissive components in our lasers is

important in perspective to reach high control on field distribution and lasing modes.[36]

4. Conclusions

Results presented here indicate that a simple, straightforward method can be developed to realize *in-vitro* nanostructured organo-mineral photonic materials by using electrospun fiber template biomineralization. The approach demonstrates how biosilification can direct the formation of components for amorphous photonics, a route never explored before which leads to the controlled generation of active optical devices such as random lasers. The transport of light in the material shows a combined effect of organic filaments and biosilica particles in supporting local field enhancement and lasing. Mimicking natural microstructures by *in-vitro* fabrication promise to greatly simplify design and manufacturing concepts for engineered light-diffusing materials.

Supporting Information

Supporting Information is available from the Wiley Online Library or from the author.

Acknowledgements

Maria Moffa and Andrea Camposeo equally contributed to this work. The research leading to these results has received funding from the European Research Council under the European Union's Seventh Framework Programme (FP/2007-2013)/ERC Grant Agreement n. 306357 ("NANO-JETS"). The support from the Apulia Regional Projects 'Networks of Public Research Laboratories' Wafitech (9) and M.I.T.T. (13) is also acknowledged. W.E.G.M. is also holder of an ERC Advanced Investigator Grant (no. 268476 "BIOSILICA").

Conflict of Interest

The authors have declared no conflict of interest.

Keywords

biosilica, electrospun nanofibers, light-scattering, random lasers

Received: August 16, 2017
Published online: October 24, 2017

[1] Y.-F. Huang, S. Chattopadhyay, Y.-J. Jen, C.-Y. Peng, T.-A. Liu, Y.-K. Hsu, C.-L. Pan, H.-C. Lo, C.-H. Hsu, Y.-H. Chang, C.-S. Lee, K.-H. Chen, and L.-C. Chen, *Nat. Nanotechnol.* **2**, 770 (2007).
[2] K. Yu, T. Fan, S. Lou, and D. Zhang, *Prog. Mater. Sci.* **70**, 1 (2015).
[3] U.G.K. Wegst, H. Bai, E. Saiz, A.P. Tomsia, and R.O. Ritchie, *Nat. Mater.* **14**, 23 (2015).
[4] A.R. Parker and H.E. Townley, *Nat. Nanotechnol.* **2**, 347 (2007).
[5] K. Liu and L. Jiang, *Nano Today* **6**, 155 (2011).
[6] H. Noh, J.K. Yang, S.F. Liew, M.J. Rooks, G.S. Solomon, and H. Cao, *Phys. Rev. Lett.* **106**, 183901 (2011).
[7] C. Jeffryes, T. Gutu, J. Jiao, and G.L. Rorrer, *ACS Nano* **2**, 2103 (2008).
[8] J.M. Galloway, J.P. Bramble, and S.S. Staniland, *Chem. Eur. J.* **19**, 8710 (2013).
[9] K. Shimizu, J. Cha, G.D. Stucky, and D.E. Morse, *Proc. Natl. Acad. Sci.* USA **26**, 6234 (1998).
[10] N. Kröger, S. Lorenz, E. Brunner, and M. Sumper, *Science* **298**, 584 (2002).
[11] J.N. Cha, K. Shimizu, Y. Zhou, S.C. Christiansen, B.F. Chmelka, G.D. Stucky, and D.E. Morse, *Proc. Natl. Acad. Sci. USA* **96**, 361 (1999).
[12] A. Scheffel, N. Poulsen, S. Shian, and N. Kröger, *Proc. Natl. Acad. Sci. USA* **22**, 3175 (2011).
[13] D. Wiersma, *Nat. Photon.* **7**, 188 (2013).
[14] M.N. Tahir, P. Théato, W.E.G. Müller, H.C. Schröder, A. Borejko, S. Faiß, A. Janshoff, J. Huth, and W. Tremel, *Chem. Commun.* **44**, 5533 (2005).
[15] D. Wiersma, *Nat. Phys.* **4**, 359 (2008).
[16] A. Tulek, R.C. Polson, and Z.V. Vardeny, *Nat. Phys.* **6**, 303 (2010).
[17] M.P. van Albada, and A. Lagendijk, *Phys. Rev. Lett.* **55**, 2692 (1985).
[18] P.E. Wolf and G. Maret, *Phys. Rev. Lett.* **55**, 2696 (1985).
[19] V.M. Alpakov, M.U. Raikh, and B. Shapiro, *Phys. Rev. Lett.* **89**, 016802 (2002).
[20] I. Horcas, R. Fernández, J. M. Gómez-Rodríguez, J. Colchero, J. Gómez-Herrero, and A. M. Baro, *Rev. Sci. Instrum.* **78**, 013705 (2007).
[21] Y.B. Lee, Y.M. Shin, J.H. Lee, I. Jun, J.K. Kang, J.C. Park, and H. Shin, *Biomaterials* **33**, 8343 (2012).
[22] A. Dong, B. Kendrick, L. Kreilgârd, J. Matsuura, M.C. Manning, and J.F. Carpenter, *Arch. Biochem. Biophys.* **347**, 213 (1997).
[23] A. Dong, P. Huang, and W.S. Caughey, *Biochemistry* **29**, 3303 (1990).
[24] M.N. Tahir, P. Théato, W.E.G. Müller, H.C. Schröder, A. Janshoff, J. Zhang, J. Huth, and W. Tremel, *Chem. Commun.* **24**, 2848 (2004).
[25] L. Sznitko, J. Mysliwiec, P. Karpinski, K. Palewska, K. Parafiniuk, S. Bartkiewicz, I. Rau, F. Kajzar, and A. Miniewicz, *Appl. Phys. Lett.* **99**, 031107 (2011).
[26] R. Zhang, S. Knitter, S. F. Liew, F. G. Omenetto, B. M. Reinhard, H. Cao, and L. Dal Negro, *Appl. Phys. Lett.* **108**, 011103 (2016).
[27] Z. Wang, X. Meng, S. H. Choi, S. Knitter, Y. L. Kim, H. Cao, V. M. Shalaev, and A. Boltasseva, *Nano Lett.* **16**, 2471 (2016).
[28] F. Hide, M. A. Diaz-Garcia, B. J. Schwartz, M. R. Andersson, and Q. B. Pei, *Science* **273**, 1835 (1996).
[29] A. K. Sheridan, G. A. Turnbull, A. N. Safonov, and I. D. W. Samuel, *Phys. Rev. B* **62**, 929 (2000).
[30] V. Fasano, A. Polini, G. Morello, M. Moffa, A. Camposeo, and D. Pisignano, *Macromolecules* **46**, 5935 (2013).
[31] L. Persano, M. Moffa, V. Fasano, M. Montinaro, G. Morello, V. Resta, D. Spadaro, P.G. Gucciardi, O.M. Maragò, A. Camposeo, and D. Pisignano, *Proc. SPIE* **9745**, 97450R (2016).
[32] H. Cao, *Waves Random Media* **13**, R1 (2003).
[33] M.B. Van der Mark, M.P. van Albada, and A. Lagendijk, *Phys. Rev. B* **37**, 3575 (1988).
[34] M. Burresi, L. Cortese, L. Pattelli, M. Kolle, P. Vukusic, D.S. Wiersma, U. Steiner, and S. Vignolini, *Sci. Rep.* **4**, 6075 (2014).
[35] F. Borghese, P. Denti, and R. Saija, *Scattering from model nonspherical particles*, 2nd Ed. Springer-Verlag Berlin Heidelberg (2007).
[36] M. Leonetti, C. Conti, and C. López, *Phys. Rev. A* **85**, 043841 (2012).